Steel and Composite Structures, *Vol. 35, No. 3 (2020) 439-447*
DOI: https://doi.org/10.12989/scs.2020.35.3.439

Thermoelastic effect on inter-laminar embedded delamination characteristics in Spar Wingskin Joints made with laminated FRP composites

P.K. Mishra*[1], A.K. Pradhan[2], M.K. Pandit[2] and S.K. Panda[1]

[1]*Department of Mechanical Engineering, Biju Patnaik University of Technology, Rourkela, Odisha, India*
[2]*School of Mechanical Sciences, Indian Institute of Technology, Bhubaneswar, India*

(*Received October 16, 2019, Revised April 12, 2020, Accepted April 24, 2020*)

Abstract. This paper presents two sets of full three-dimensional thermoelastic finite element analyses of superimposed thermo-mechanically loaded Spar Wingskin Joints made with laminated Graphite Fiber Reinforced Plastic composites. The study emphasizes the influence of residual thermal stresses and material anisotropy on the inter-laminar delamination behavior of the joint structure. The delamination has been pre-embedded at the most likely location, i.e., in resin layer between the top and next ply of the fiber reinforced plastic laminated wingskin and near the spar overlap end. Multi-Point Constraint finite elements have been made use of at the vicinity of the delamination fronts. This helps in simulating the growth of the embedded delamination at both ends. The inter-laminar thermoelastic peel and shear stresses responsible for causing delamination damage due to a combined thermal and a static loading have been evaluated. Strain energy release rate components corresponding to the Mode I (opening), Mode II (sliding) and Mode III (tearing) of delamination are determined using the principle of Virtual Crack Closure Technique. These are seen to be different and non-self-similar at the two fronts of the embedded delamination. Residual stresses developed due to the thermoelastic anisotropy of the laminae are found to strongly influence the delamination onset and propagation characteristics, which have been reflected by the asymmetries in the nature of energy release rate plots and their significant variation along the delamination front.

Keywords: delamination; strain energy release rate; Spar Wingskin Joint; thermoelastic; virtual crack closure technique

1. Introduction

Adhesive bonded joint structures made with laminated FRP composites find significant importance in various real world applications such as aircraft, space and automobile industries. However, designing these types of joint structures is quite complex due to the limited characteristics of the composite laminated adherends with a bi-material interface that usually have low inter-laminar or out of plane strengths. The inter-laminar or out of plane stresses induced near the bond-line of joint structures may cause delamination in the laminated adherends. In addition, adhesive bonded joints may also fail due to adhesive and cohesive failures. Hence, an exact three-dimensional (3D) analysis is needed for a better understanding of the joint stress fields, failure/damage initiation and ultimately its propagation in real life applications.

Adhesive bonded Spar Wingskin Joint (SWJ) is one of the joint structures used in practical applications like integral wing design and manufacture (Lackman *et al*. 1980 - Mishra *et al*. 2016). Due to specific need and demand, the finite element method (FEM) is widely used for accurate and better analyses of an adhesively bonded joint. Examples of finite element investigations of adhesively bonded composite joints include (Tong 1998), (Krueger *et al*. 2003), (Grant *et al.* 2009), (Banea and da Silva 2009), (Kharazana *et al.* 2014), (Benchiha and Madani 2015), (Elhannani *et al.* 2016), (Xu *et al.* 2019) and others. The literature confirm that standard FE codes can analyze the adhesively bonded joints with or without failures/damages subjected to various loading conditions. Different joint configurations can be analyzed quickly and accurately and pre-and post-processing of each FE model can take merely a few hours/days. Further, the high stress gradients of adhesively bonded joints at the overlap region which dependent on mesh refinement can also be realized.

In practice, the adhesive bonded joints experience mechanical (structural) loading as well as thermal loadings. As the adhesive bonded composite joints comprise of materials having different mechanical and thermal properties, the resulting thermal strains in the joint structures may cause severe stresses. However, these thermal stresses cannot be avoided since more than hundred degrees of temperature change (fabrication and room temperature) occurs during fabrication of the joints made with composite laminates. These stresses lead to the initiation and further propagation of delamination/adhesion failure in joints. The mechanism of delamination/adhesion failure growth depends on residual stresses along with stacking sequence of fibers, mismatch of coefficient of thermal expansion and material anisotropy between the plies and the matrix of the laminates.

Hence, study on delamination/adhesion failure initiation and its propagation in composite laminated joints subjected to thermoelastic anisotropy are essential. Kakei *et al.* (2016)

*Corresponding author, Ph.D.
E-mail: capgs.pkmishra@bput.ac.in

ISSN: 1229-9367 (Print), 1598-6233 (Online)

investigated both experimentally and numerically thermoelastic stress effects on delamination propagation for a woven glass epoxy composite material subjected to cyclic loading. They concluded that the measured delamination growth rate results were consistent with that of simulation results. Francavilla *et al.* (2016) proposed a theoretical model to study the fracture behaviour of bolted T-stub subjected to monotonic loading. They verified the accuracy of the proposed model by comparing it with experimental results. Moradi-Dastjerdi *et al.* (2017) used a mesh free method to investigate the thermoelastic behaviour of functionally graded carbon nanotube reinforced composite cylinder. In mesh free analysis, the displacement field and the temperature has been calculated using moving least squares shape functions. Temperature and hoop stress distribution of thick composite cylinders were affected by the graphene distribution. Distribution and volume fraction of graphene in the composite cylinders has also affect on the natural frequencies (Moradi-Dastjerdi *et al.* 2019). Sassi *et al*. (2018) presented a new experimental method to measure the kinetic damage, deformation and temperature in adhesive bonded composite joints. An infrared camera was used to monitor the surface temperature of the specimen. The stress-strain behaviour of the specimen was affected by the increase in strain rate and the stress concentration appears in the adhesive area as the temperature increases at that location.

Composites are used in space and low temperature mechanical equipment. Therefore, the mechanical behaviour of fiber-reinforced epoxy must be observed. Shokrieh *et al.* (2012) investigated the tensile failure behaviour under thermo-mechanical static load of glass/epoxy laminated composite. Nguyen *et al.* (2012) studied the time-dependent behaviour of steel/CFRP double strap joints subjected to combine thermal and mechanical loading. The joints were subjected to the cyclic thermal loading between 20℃ and 50℃. Kumar *et al.* (2005) studied the composite materials subjected to thermal and thermo-mechanical loadings considering the effect of fiber orientation of the structure. They found that the thermal stress is pre-dominant compared to that of mechanical stress. Benchiha *et al.* (2015) analyzed the adhesive shear stress distribution of a single lap bonded joint using the finite element method and found that shear stress was maximum at the defect surface because of high stress concentration factor. Elhannani *et al.* (2016) used 3D nonlinear finite element method to analyze the stress distribution in adhesively bonded aluminium adherends and optimize the geometrical parameters of the joint. Cracking of composite material and micro buckling of the z-pin mainly occur in z-pin surrounded with composite material. The integrity and strength of the structural joint are improved at elevated temperature (Byrd *et al*. 2006). Aramid nonwoven fabrics can be used to improve the toughness value for mode-I fracture of carbon fiber composites. These fabrics also increase the impact of strength and inter-laminar shear strength (Beylergil *et al*. 2019).

In most of the real life physical problems, it has long been recognized that mechanical and thermal fields are coupled. Thermal effects might be treated as important when the system undergoes low or high temperature gradients. The high local stress fields could be developed in a composite laminate due to mismatch of thermal strain and ultimately may affect the strength/integrity of the structure.

From above discussions, it is concluded that although a good amount of literature is available on delamination damages in FRP composite laminates, very little has been reported in analyzing thermal residual stress effects on fracture behaviour of a realistically induced inter-laminar embedded delamination due to sequential thermo-mechanical loading. As these damage mechanisms are complex in nature, it is essential to model both delamination initiation and its propagation. Therefore, in depth analysis of embedded delamination by considering curing stress effect subjected to thermo-mechanical loading is a realistic example.

In view of the above, in the present case, mixed-mode interlaminar fracture behaviour in adhesive bonded SWJs made with FRP laminated composites have been investigated by considering the interaction of thermal residual stress (experienced during the curing stages in the manufacturing of FRP laminated composites) and a subsequent transverse mechanical loading. For this, two sets of simultaneous coupled field finite element analyses have been conducted to evaluate the displacements and stresses for the embedded delaminations at the overlap region of the spar-wingskin. Composite material anisotropy/ heterogeneity and varying thermoelastic stresses in the SWJ pose difficulties. However, careful and judicious use of finite element simulation with physically meaningful and realistic assumptions will make the analysis results absolutely idealistic. Hence, superposition finite element procedure in conjunction with the virtual crack closure technique (VCCT) based on linear elastic fracture mechanics (LEFM) the concept is employed to evaluate the individual mode of strain energy release rates (SERR) in the SWJ during interlaminar delamination propagation.

2. Delamination at crack front

In the application of LEFM to various engineering problems, the most important and necessary aspect is to determine the singular stress field at the crack tip and express it in terms of individual modes of stress intensity factors (SIF). For isotropic monolithic materials, these amplitudes generally are square root stress singular. As the strain energy available in the crack tip region is finite, the finite element energy method may be successfully applied. Thus, convergence criteria of energy release rate are successfully attained. Use of SIF to quantify studies on crack growth is well established for isotropic materials.

However, composites are generally more complex due to the presence of singularities of the stress field at the crack tip. Characterization of crack growth in composite materials is mostly dealt with the principle of energy conservation. Interface/interlaminar crack growth in orthotropic composite materials are quite complex due to the mismatch of material properties present at the interface/laminate (Rice 1988 and Hong *et al.* 1989).

In addition, the inadequacies in analytical studies for complex geometrical dimensions and predominant boundary conditions lead to finite element approach that simplifies the crack growth. Therefore, to solve more practical problems related to fracture mechanics, the finite element method for SERR has readily been used to evaluate crack propagation and assess the effect of different parameters viz. crack geometry, crack location, applied state of stresses, constraint conditions, material properties, etc.

2D or 3D elasticity theories are not well defined for the individual SERR components at the crack front in bimaterial interfaces. This is occurring due to the presence of oscillatory stress and displacement fields at the crack front. Again, uniform change in temperature during curing of the laminate will induce the thermal residual stresses. The mismatch of thermoelastic material properties in the laminate made of different plies, orientations would result in mixed-mode behaviour under thermo-mechanical loading. Hence, a fully 3D fracture analysis is essential for comprehensive study at the delamination front.

To deal with composite laminates subjected to delaminations, it is preferable to use total energy release rate instead of individual components of SERR. In the present study, sub-laminate techniques have been used to model the SWJ structure and evaluate the individual components of the SERR along the delamination damage fronts. The analysis domain of the joint structure has been divided into three sub-parts i.e., the spar (top), wingskin (bottom) and the epoxy adhesive layer (middle). The spar and wingskin sub-laminate are made up of FRP composite (graphite/epoxy or glass/epoxy or boron/epoxy). The middle part is made up of isotropic epoxy adhesive which joins the spar and wingskin. Delamination propagation characteristics in the joint structure have been analysed using well defined finite element based VCCT method. The most significant advantage of this method is that using a single FE run, the three components of the SERR can be determined for delamination (crack) problems.

3. Strain energy release rate (SERR) evaluation

In general, crack propagation can occur in three different ways i.e., opening mode (Mode I), in plane shearing mode (Mode II) and out of plane tearing mode (Mode III). However, in composite materials, the delamination (crack) propagation can occur either in any one of the above modes or a combination of them which is known as mixed-mode (Wilkins *et al.* 1982). Individual modes of SERR along the delamination fronts are evaluated based on concepts of LEFM developed by (Irwin, 1957) and modified by (Rybicki and Kanninen, 1977) subjected to the thermo-mechanical loading. The energy released during crack propagation from length ‘a’ to ‘a + Δa’ due to sequential thermo-mechanical loading is equal to work needed to close the crack from length ‘a + Δa’ to ‘a’ as shown in Fig. 1.

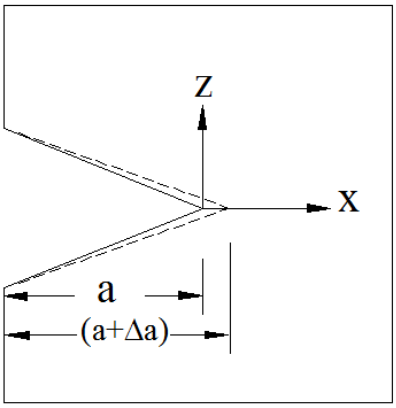

Fig. 1 Schematic of crack growth

$$W = \frac{1}{2}\int_0^{\Delta a} [\sigma_M(x) + \sigma_T(x)\ ][\delta_M(x - \Delta a) + \delta_T(x - \Delta a)\ ]\ dx \quad (1)$$

where the subscripts ‘M’ and ‘T’ denote the mechanical and thermal effects, respectively. δ(x-Δa) is the crack opening displacement between the top (1st ply) and bottom (2nd ply) delaminated surface as shown in Fig. 2. σ(x) is the required stress at the crack front that close the delaminated area. Mode I is produced due to the crack opening, Mode II due to the in-plane shear and Mode III due to the out-of-plane shear component at the crack front. So, the energy release rate is obtained expressed as

$$G = \lim_{\Delta a \to 0}\left(\frac{W}{\Delta a}\right) \quad (2)$$

3.1 Computation of SERR using VCCT

Computation of SERRs using the VCCT method in the SWJ made with laminated FRP composite at the delamination front (PQ front) is shown in Fig. 2. SERR has been evaluated with the increase of delamination length by ‘Δa’ for the delamination front PQ and also for MN front. Near the delamination fronts, 3D eight nodded layered volume elements known as SOLID 185 has been used with the size of [(Δa× Δa) × total layer thickness]. This has been clearly described in Section 5. The VCCT method requires a sufficiently identical and uniform size of layered volume elements along the delamination fronts across the width of the wingskin. For accurate and qualitative fracture analysis of delaminated structures, VCCT method is most preferable as it has the advantage of mode separation of SERRs. For implementation of VCCT, finer and symmetric FE mesh should be provided along the damage front. The three modes of SERRs (Mode I, Mode II, and Mode III) are given as

$$G_I = \frac{1}{2\Delta A}\ [Z_{Mf} + Z_{Tf}](w_T - w_B) \quad (3)$$

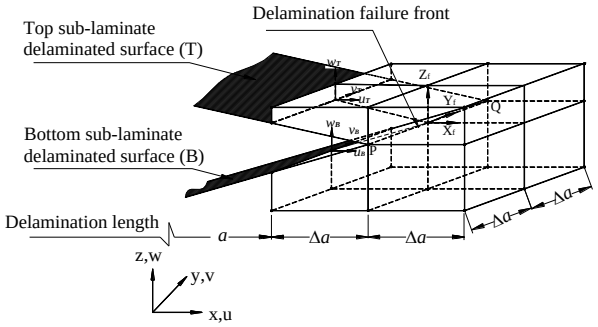

Fig. 2 FE model at delamination front PQ in the SWJ

$$G_{II} = \frac{1}{2\Delta A}\left[X_{Mf} + X_{Tf}\right](u_T - u_B) \quad (4)$$

$$G_{III} = \frac{1}{2\Delta A}\left[Y_{Mf} + Y_{Tf}\right](v_T - v_B) \quad (5)$$

where, subscripts T and B denote the top and bottom delaminated surfaces, respectively (Fig. 2). $[u_T, v_T, w_T]$ and $[u_B, v_B, w_B]$ represent the nodal displacements corresponding to the top and the bottom delaminated surfaces, respectively situated behind the delamination front. Here, the virtually closed area, $\Delta A = \Delta a \times \Delta a$ and Z_f, X_f and Y_f are denoted as the forces for opening, sliding and tearing mode, respectively. Subscripts 'M' and 'T' are the mechanical and the thermal effect parameters as stated earlier. These forces hold the nodes at the tip of the delamination front together thereby preventing it from further propagation. Magnitudes of these forces are evaluated by using MPC elements. G_I, G_{II} and G_{III} values are calculated by varying values of delamination length '2a'. Delamination growth behaviour of the joint would be indicated for the rate of variation of these values. The total SERR considering the sequential thermo-mechanical effects can then be expressed as

$$G_{Total} = G_I + G_{II} + G_{III} \quad (6)$$

4. SWJ geometry and material constants

The SWJ specimen made with laminated FRP composite adherends for integral fuselage and wing construction is shown in Fig. 3. The sectional portion is shown by planes AA, BB and CC of the SWJ consider for analysis. The dimensions of the joint considered are given as follows (Mishra *et al.* 2016):

Half span length, L = 60 mm, spar thickness, t_1 = 0.5 mm, wingskin thickness, t_2 = 2 mm, SWJ width, W = 25 mm, spar overlap length, c = 15 mm, g = 8 mm, e = 2 mm, b = 21 mm, h = 14 mm. The spar and the wingskin are made of symmetric cross ply laminates ([0/90]s) with ply thickness 0.125 mm and 0.5 mm, respectively.

A comprehensive 3D FE analysis on SWJ reveals that the delamination failure initiates at the interface of 1st and 2nd plies of the wingskin adherend. The location is near the toe end of the spar wingskin overlap region Mishra et al. (2016). The schematic geometry of the SWJ along with embedded delamination of varying sizes, type of loading and boundary conditions is shown in Fig. 4. Referring to Figure 3, symmetric boundary conditions have been applied to Sections AA and CC and no displacements (constrained end) condition have been applied to Section BB. In the present work, two separate sets of 3D finite element analyses have been carried out for each SWJ configuration. First one is for mechanical loading (without any thermal loading) only i.e. a uniformly distributed transverse load of magnitude 40 N/mm along the width of the wingskin at the free end of the SWJ (Jena, (1993)). Second set by considering both above mentions mechanical and thermal (Uniform temperature change) load sequentially to take into account of thermal residual stress effects.

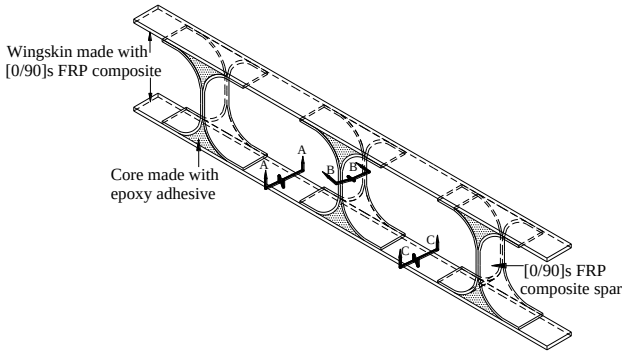

Fig. 3 SWJ used for integral fuselage and wing structural construction of aircraft (Analysis domain: AA, BB and CC sectional planes)

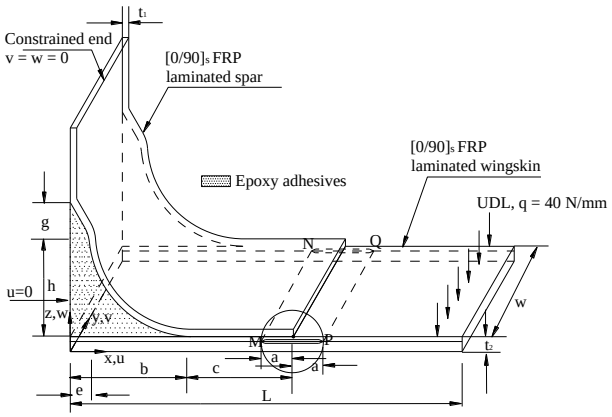

(a) Symmetric half sectional view of the SWJ along with through-the-width embedded delamination

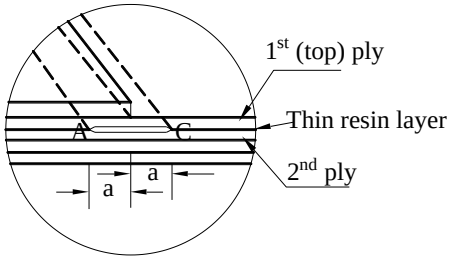

(b) Zoomed view of the overlap end of the SWJ

Fig. 4 Geometry, loading and boundary condition of the SWJ with embedded delamination

Table 1 Mechanical properties of FRP composites

Properties	Graphite/epoxy	Glass/epoxy	Boron/epoxy
E_x (GPa)	181.0	38.60	207.00
$E_y = E_z$ (GPa)	10.30	8.27	18.63
$v_{xy} = v_{xz}$	0.28	0.25	0.27
v_{yz}	0.30	0.27	0.35
$G_{xy} = G_{xz}$ (GPa)	7.17	4.14	4.50
G_{yz} (GPa)	4.00	4.00	3.45
Thermal Properties (Co-efficient of thermal expansion)			
α_x	0.025×10^{-6}/℃	7×10^{-6}/℃	6.1 $\times 10^{-6}$/℃
$\alpha_y = \alpha_z$	22.5×10^{-6}/℃	21 $\times 10^{-6}$/℃	30 $\times 10^{-6}$/℃

Table 2 Mechanical properties of interfacial 6376 epoxy adhesive

E_x (GPa)	3.89
G (GPa)	1.82
v	0.37
α (Coeff. of thermal expansion)	44×10^{-6}/℃

Table 3 Temperature state of thermal loading

Curing temperature	140 ℃
Room temperature	30 ℃

Through-the-width delaminations of 0.02 mm thick have been presumed to be embedded in the resin layer between the first and second plies of the wingskin adherend. In the present analysis, five different embedded delamination lengths of magnitudes 2a = 2, 4, 6, 8 and 10 mm are simulated to be symmetrically present about the overlap end of the SWJ. The thermoelastic material properties used for FRP composites and the resin layer, respectively are listed in Tables 1 and 2. Uniform thermal loading (temperature state) to induce initial residual stresses has been displayed in Table 3. It is assumed to be stress free for the initial curing state temperature of the SWJ.

5. Finite element analysis

In the present work, 3D finite element techniques have been adopted to investigate the fracture behaviour of interlaminar delamination at crack fronts in the SWJ subjected to the thermo-mechanical loading using FE software of ANSYS 18.0 (Ansys Parametric Design Language (APDL)). Two sets of numerical analysis have been carried out for each SWJ configuration i.e., one considering mechanical loading only and another considering sequential thermo-mechanical loading (residual stress effect). The thermal loading (uniform temperature change) occurs during curing of manufacturing of FRP composite laminates. The thermoelastic characteristics of delamination propagation have been compared for different configuration and materials results.

3D eight nodded layered volume element SOLID 185 have been used for modelling of the spar and wingskin adherends ply by ply. 3D eight nodded structural volume element SOLID 185 has been used to model the adhesive layer present between the spar and wingskin overlap. Sub-laminate modelling technique have been used to model the various parts of the SWJ as shown in Fig. 5. The embedded delamination is simulated to be present symmetrically at the spar wingskin overlap region. The FE mesh is shown in Fig. 6.

The SERR method of VCCT based on sound energy balance principle (Rybicki and Kanninen 1977) has been widely accepted as the standard fracture parameter and same has been adopted as it is convenient for the joint structure considered. Multi point constraint (MPC) and CONTACT 178 (gap) elements available with ANSYS 18.0 have been provided at the nodes of the delaminated interfaces of the joint.

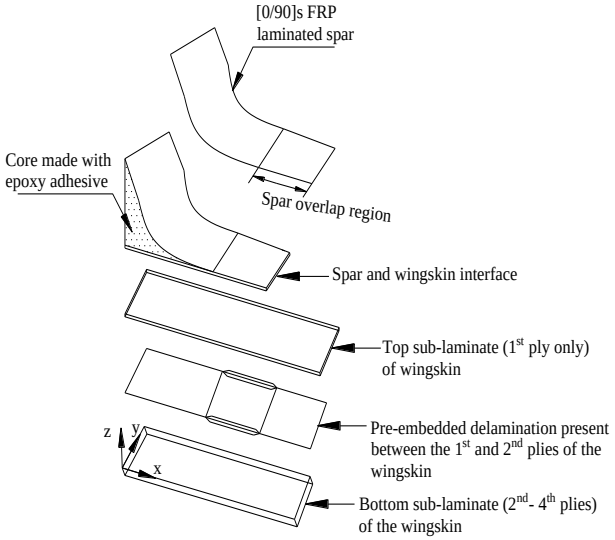

Fig. 5 Sub-laminate configuration of the SWJ indicating pre-embedded delamination

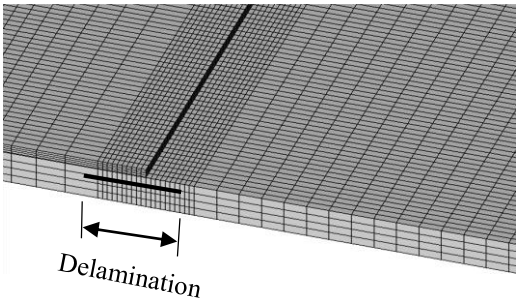

Fig. 6 FE mesh of the SWJ (damage front portion)

By sequential removal of these MPC elements, progressive delamination propagation has been simulated. The gap elements are used to ensure prevention of inter-penetration of the delaminated layers without any frictional effect. The convergence of the present SWJ model has been achieved by considering error analyses and mesh refinements so that limit of variation of SERRs along the delamination fronts to be 0.001%. Accordingly, one fourth of ply thickness of SWJ at the delamination front and considerably coarse elements away from damage front have been used.

6. Results and discussion

The SERR (G_I, G_{II} and G_{III}) distributions along the two delamination fronts in the SWJ have been evaluated by considering with and without the thermal residual stress effects. The SERR results for mechanical loading only and a sequential thermo-mechanical loading considering residual thermal stress effects are defined by the subscripts 'M' and 'TM', respectively.

6.1 Variations of SERRs along the MN and PQ delamination fronts

This section discusses the SERR variations along the delamination fronts MN and PQ for the SWJ made with graphite/epoxy laminate. Results are shown with and without considering the effect of thermal residual stresses for the out of plane transverse load (substeps) applied at the edges of the wing-skin laminate. Delamination propagation characteristics due to the effects of curing stresses have been indicated by the mismatch of the asymptotic energy release rate curves along the delamination fronts. Embedded delamination and its growth with an increase in size may cause a reduction in load carrying capability and finally catastrophic failure. From the SERR plots (Figs. 7 and 8), it is observed that the effects of residual stresses are much more prominent over the region of maximum values of SERR components at the centre of the delamination fronts. These increase in SERR values have significant importance for the delamination damage analysis of composite joints. The existence of initial residual stresses causes an increase in SERR parameters and subsequently intends for premature laminate failure. Figs. 6 and 7 indicate that the Mode I delamination fracture, i.e., G_I is significantly affected by the initial residual stresses for both the delamination fronts MN and PQ. It is also observed that the rate of propagation (SERR values) in delamination front, PQ is faster compared to that at delamination front MN for all delamination lengths with or without curing stress effect. This phenomenon may be due to the geometry, loading and boundary conditions of the delamination fronts (MN and PQ) in the joint structure.

6.2 Comparison of total SERR (G_T) along the MN and PQ delamination fronts

The results found in the previous section lead to a phenomenon that the delamination propagation occurs in a mixed mode manner for the SWJ with and without considering the effect of thermal residual stresses. Though, G_I is the most dominant mode for the SWJ considered, evaluation of total SERR (G_T) is essential for a comprehensive assessment of the structural strength and integrity.

Fig. 9 shows the variations of G_T for the two delamination fronts MN and PQ, respectively by considering with and without the effect of thermal residual stress. It is seen that the rate of propagation (G_T) in delamination front PQ is higher compared to that at delamination front MN for all delamination lengths. However, G_T is more prominent with thermo-mechanical loading than that of mechanical loading only.

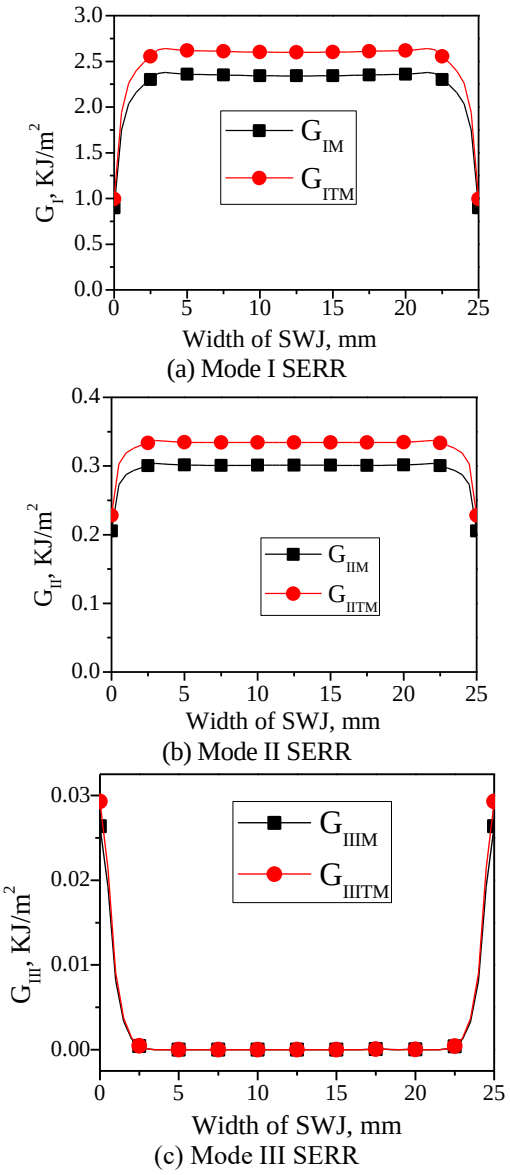

Fig. 7 Variations of SERR components along the delamination front MN (with or without thermal residual stress effect)

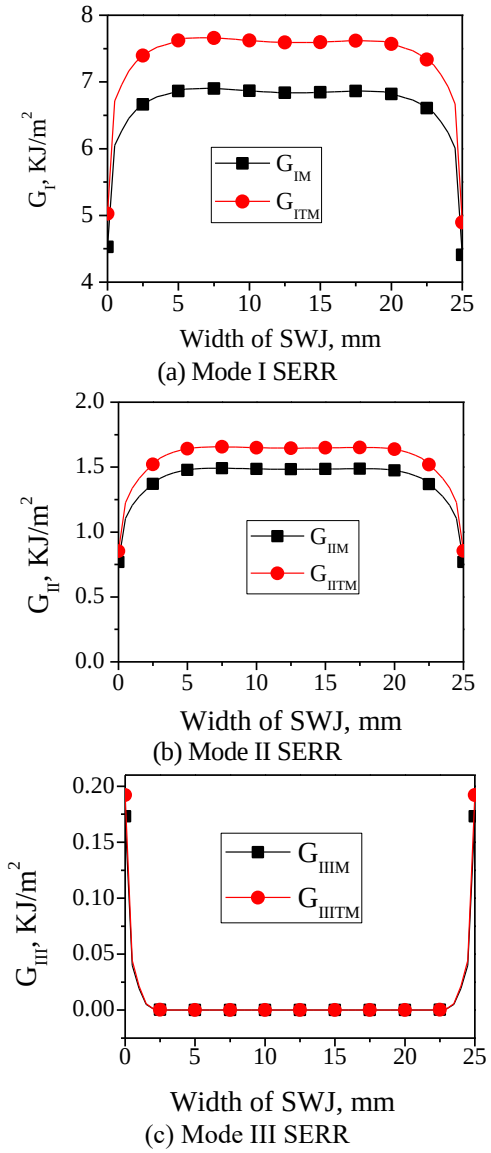

Fig. 8 Variations of SERR components along the delamination front PQ (with or without thermal residual stress effect)

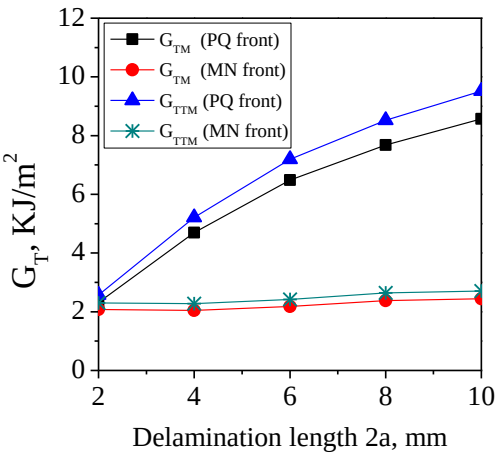

Fig. 9 Variations of total SERR (G_T) in delamination fronts MN and PQ (with or without thermal residual stress effect)

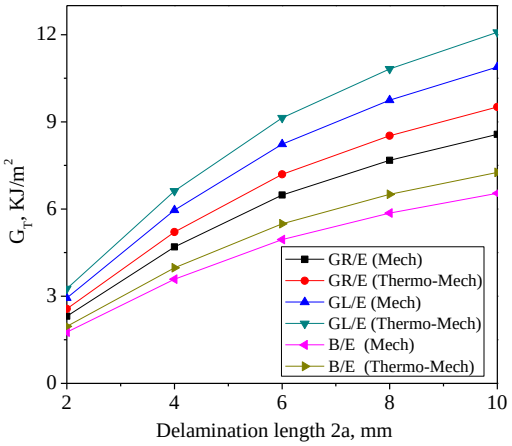

Fig. 10 Variations of total SERR (G_T) in delamination fronts PQ (For individual FRP laminate)

6.3 Effect of thermal residual stresses and material anisotropy on SERR distribution

Effect of thermal residual stresses and material anisotropy on delamination propagation behaviour, a comparison of total SERRs have been made along the delamination front for SWJ made of graphite/epoxy (GR/E), glass/epoxy (GL/E) and boron/epoxy (B/E) FRP composites laminate. Geometry, loading and constraint conditions have been kept the same as described in earlier sections. Both mechanical and thermo-mechanical effects on total SERR (G_T) distribution at embedded delamination fronts for GR/E, GL/E and B/E laminates have been plotted in Fig. 10. It is seen that the spread over of G_T value for GL/E laminate is maximum, followed by GR/E and B/E laminate, respectively.

This may be due to the influence coefficients between the longitudinal and transverse directions and orthotropic modulus ratio. The significant difference between the mechanical and thermo-mechanical effects on delamination propagation has been indicated by the mismatch in SERR plots of the SWJ laminates. Also, the reasonable difference between the maximum and minimum G_T values for the individual FRP laminate can be accounted to the thermoelastic heterogeneity and mismatch of thermal expansion coefficients.

7. Conclusions

The analysis of embedded delaminations in SWJ made with FRP composite laminates subjected to out of plane transverse loading by considering with or without the effects of thermal residual stress effect have been performed using VCCT method of SERR as a fracture parameter (LEFM). The results obtained from the detail investigations have been summarized below.

- Presence of thermal residual stresses significantly affect the delamination and its propagation. Although, variations of SERRs (G_I, G_{II} and G_{III}) are

symmetric along the delamination front, they are not constant. Hence, a full three dimensional analysis is essential to be conducted when residual thermal stress effects are to be taken into consideration.

- Individual modes of strain energy release rates indicate non-self-similar delamination/crack growth at the delamination fronts of the SWJ for both mechanical and thermo-mechanical analysis.
- The residual thermal stresses increase the rate of delamination damage to the joint in addition to those caused due to mechanical loading. This added damage degrades the strength and stiffness of the joint structure significantly.
- It is concluded that the driving force for Mode I delamination fracture, i.e., G_I is significantly affected by the initial thermal residual stresses for both the delamination fronts MN and PQ. It is also seen that the rate of propagation at delamination front PQ is higher compared to that at MN front for all delamination lengths with or without curing stress effect.
- The difference in total strain energy rate 'G_T' with and without considering the effects of thermal residual stresses among boron/epoxy, graphite/epoxy and glass/epoxy laminates are due to the mismatch of thermal expansion coefficients and mutual influence coefficients and anisotropy modulus ratio among laminae. It is observed that the G_T value for glass/epoxy is maximum, followed by graphite/epoxy and boron/epoxy, respectively.

References

Banea, M.D. and da Silva, L.F. (2009), "Adhesively bonded joints in composite materials: an overview", *Proceedings of the Institution of Mechanical Engineers, Part L: Journal of Materials: Design and Applications*, **223**(1), 1-18.

Benchiha, A. and Madani, K. (2015), "Influence of the presence of defects on the stresses shear distribution in the adhesive layer for the single-lap bonded joint", *Struct. Eng. Mech.*, **53**(5), 1017-1030. https://doi.org/10.12989/sem.2015.53.5.1017.

Beylergil, B., Tanoglu, M. and Aktas, E. (2019), "Mode-I fracture toughness of carbon fiber/epoxy composites interleaved by aramid nonwoven veils", *Steel Compos. Struct.*, **31**(2), 113-123. https://doi.org/10.12989/scs.2019.31.2.113.

Byrd, L.W. and Birman, V. (2006), "Effect of temperature on stresses and delamination failure of z-pinned joints", *Int. J. Mech. Sci.*, **48**(9), 938-949. https://doi.org/10.1016/j.ijmecsci.2006.03.014.

Cope, R.D. and Pipes, R.B. (1982), "Design of the composite spar-wingskin joint", *Composites*, **13**(1), 47-53. https://doi.org/10.1016/0010-4361(82)90170-7.

Elhannani, M., Madani, K., Mokhtari, M., Touzain, S., Feaugas, X., and Cohendoz, S. (2016), "A new analytical approach for optimization design of adhesively bonded single-lap joint", *Struct. Eng. Mech.*, **59**(2), 313-326. http://dx.doi.org/10.12989/sem.2016.59.2.313.

Francavilla, A.B., Latour, M., Piluso, V. and Rizzano, G. (2016), "Bolted T-stubs: A refined model for flange and bolt fracture modes", *Steel Compos. Struct.*, **20**(2), 267-293. https://doi.org/10.12989/scs.2016.20.2.267.

Gillespie Jr, J.W. and Pipes, R.B. (1978), "Behavior of integral composite joints-finite element and experimental evaluation 1", *J. Compos. Mater.s*, **12**(4), 408-421. https://doi.org/10.1177/002199837801200406.

Grant, L.D.R., Adams, R.D. and da Silva, L.F. (2009), "Experimental and numerical analysis of single-lap joints for the automotive industry", *Int. J. Adhesion Adhesives*, **29**(4), 405-413. https://doi.org/10.1016/j.ijadhadh.2008.09.001.

Hong, S. and Liu, D. (1989), "On the relationship between impact energy and delamination area", *Exp. Mech*., **29**(2), 115-120. https://doi.org/10.1007/BF02321362.

Irwin, G.R. (1957), "Analysis of stresses and strains near the end of a crack transversing a plate", *T. ASME, J. Appl. Mech.*, **24**, 361-364.

Jena, B. (1993), "Analysis of Adhesive-Bonded Joints in FRP Composite Laminates and Tubes", (Doctoral dissertation, IIT, Kharagpur).

Kairouz, K.C. and Matthews, F.L. (1993), "Strength and failure modes of bonded single lap joints between cross-ply adherends", *Composites*, **24**(6), 475-484. https://doi.org/10.1016/0010-4361(93)90017-3.

Kakei, A., Epaarachchi, J.A., Islam, M., Leng, J. and Rajic, N. (2016), "Detection and characterisation of delamination damage propagation in Woven Glass Fibre Reinforced Polymer Composite using thermoelastic response mapping", *Compos. Struct.*, **153**, 442-450. https://doi.org/10.1016/j.compstruct.2016.06.044.

Kharazan, M., Sadr, M.H. and Kiani, M. (2014), "Delamination growth analysis in composite laminates subjected to low velocity impact", *Steel Compos. Struct.*, **17**(4), 387-403. http://dx.doi.org/10.12989/scs.2014.17.4.387

.Krueger, R., Minguet, P.J. and O'Brien, T.K. (2003). "Implementation of interlaminar fracture mechanics in design: an overview".

Kumar, R.R., Vinod, G., Renjith, S., Rajeev, G., Jana, M.K. and Harikrishnan, R. (2005), "Thermo-structural analysis of composite structures", *Mater. Sci. Eng.*: A, **412**(1-2), 66-70. https://doi.org/10.1016/j.msea.2005.08.065.

Lackman, L.M., O'brien, W.L. and Loyd, M.S. (1980), "Advanced composites integral structures meet the challenge of future aircraft systems", *Fibrous composites in structural design*. Springer, Boston, MA.

Mishra, P.K., Pradhan, A.K. and Pandit, M.K. (2016), "Inter-laminar delamination analyses of Spar Wing-skin Joints made with flat FRP composite laminates", *Int. J. Adhesion Adhesives*, **68**, 19-29. ttps://doi.org/10.1016/j.ijadhadh.2016.02.001.

Moradi-Dastjerdi, R. and Payganeh, G. (2017), "Thermoelastic dynamic analysis of wavy carbon nanotube reinforced cylinders under thermal loads", *Steel Compos. Struct.*, **25**(3), 315-326. https://doi.org/10.12989/scs.2017.25.3.315

.Moradi-Dastjerdi, R. and Behdinan, K. (2019), "Thermoelastic static and vibrational behaviors of nanocomposite thick cylinders reinforced with graphene", *Steel Compos. Struct.*, **31**(5), 529-539. https://doi.org/10.12989/scs.2019.31.5.529.

Nguyen, T.C., Bai, Y., Al-Mahaidi, R. and Zhao, X.L. (2012), "Time-dependent behaviour of steel/CFRP double strap joints subjected to combined thermal and mechanical loading", *Compos. Struct.*, **94**(5), 1826-1833. https://doi.org/10.1016/j.compstruct.2012.01.007.

Panigrahi, S.K. and Pradhan, B. (2009), "Development of load coupler profiles of spar wingskin joints with improved performance for integral structural construction of aircraft wings", *J. Reinf. Plast. Comp.*, **28**(6), 657-673. https://doi.org/10.1177/0731684407086594.

Rice, J. (1988), "Elastic fracture mechanics concepts for interfacial

cracks", *J. Appl. Mech.*, **55**(1), 98-103. https://doi.org/10.1115/1.3173668.

Rybicki, E.F. and Kanninen, M.F. (1977), "A finite element calculation of stress intensity factors by a modified crack closure integral", *Eng. Fract. Mech.*, **9**(4), 931-938. https://doi.org/10.1016/0013-7944(77)90013-3.

Sassi, S., Tarfaoui, M., and Yahia, H.B. (2018), "Thermomechanical behavior of adhesively bonded joints under out-of-plane dynamic compression loading at high strain rate", *J. Compos. Mater.s*, **52**(30), 4171-4184. https://doi.org/10.1177/0021998318777048.

Shokrieh, M.M., Torabizadeh, M.A. and Fereidoon, A. (2012), "Progressive failure analysis of glass/epoxy composites at low temperatures", *Strength of Materials*, **44**(3), 314-324. https://doi.org/10.1007/s11223-012-9384-3.

Tong, L. (1998), "Failure of adhesive-bonded composite single lap joints with embedded cracks". *AIAA J.*, **36**(3), 448-456.

Wilkins, D.J., Eisenmann, J.R., Camin, R.A., Margolis, W.S. and Benson, R.A. (1982), "Characterizing delamination growth in graphite-epoxy", *Damage in Composite Materials: Basic Mechanisms, Accumulation, Tolerance, and Characterization*. ASTM International.

Xu, Y., Chen, D.M., Zhu, W., Li, G. and Chattopadhyay, A. (2019). "Delamination identification of laminated composite plates using measured mode shapes", *Smart Struct. Syst.*, **23**(2), 195-205. http://dx.doi.org/10.12989/sss.2019.23.2.195.

CC